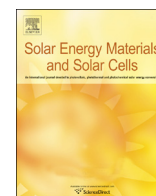




ELSEVIER

Contents lists available at ScienceDirect

Solar Energy Materials & Solar Cells

journal homepage: www.elsevier.com/locate/solmat

Bandgap grading and Al_{0.3}Ga_{0.7}As heterojunction emitter for highly efficient GaAs-based solar cells

Sun-Tae Hwang^{a,b}, Soohyun Kim^a, Hyeunseok Cheun^a, Hyun Lee^a, Byungho Lee^b,
Taehyun Hwang^b, Sangheon Lee^b, Wonki Yoon^a, Heon-Min Lee^a, Byungwoo Park^{b,*}

^a Materials & Devices Advanced Research Institute, LG Electronics, Seoul 06763, Republic of Korea

^b WCU Hybrid Materials Program, Department of Materials Science and Engineering, Research Institute of Advanced Materials, Seoul National University, Seoul 08826, Republic of Korea

ARTICLE INFO

Article history:

Received 11 January 2016

Received in revised form

1 June 2016

Accepted 7 June 2016

Available online 20 June 2016

Keywords:

GaAs solar cells

Heterojunction

Bandgap grading

ABSTRACT

Both an Al_{0.3}Ga_{0.7}As heterojunction in the *p*-type emitter and a bandgap-graded layer in the *n*-type light absorbing base were employed in the GaAs-based solar cells. The simulation by AFORS-HET (Helmholtz-Zentrum Berlin) confirmed that the Al_{0.3}Ga_{0.7}As heterojunction enhanced the open-circuit voltage (V_{oc}) by ~2%, and the *n*-type bandgap grading increased the fill factor by ~1%, respectively. The increased power conversion efficiency by ~3% supported the simulation results. An additional efficiency gain was obtained by the shape optimization of the band bending in the 80-nm compositional profile, increasing V_{oc} up to 1.103 V. The cell with the anti-reflective coating exhibited high performance with a power conversion efficiency of 28.7% under 1 sun illumination, close to the world record of 28.8%.

© 2016 Elsevier B.V. All rights reserved.

1. Introduction

Enormous efforts have been directed for decades to accomplish high power-conversion efficiency and low fabrication cost with various light harvesting materials, to make solar cells more competitive with the conventional energy sources [1–9]. Among these materials, group III–V compound semiconductors, including gallium arsenide (GaAs), have been considered as the best choice for the highest conversion efficiency of all types of the solar cells, owing to their superior absorption coefficient, carrier mobility, and direct bandgap [1–4]. However, their applications are usually limited only to the concentrated photovoltaics (CPV) or space applications because the GaAs substrates are quite expensive [10,11]. To reduce the manufacturing cost, many researchers have strived to recycle the substrates, called as epitaxial lift-off (ELO) [12–16]. The solar cells by the ELO process have additional advantages of the open-circuit voltage (V_{oc}) and short-circuit current density (J_{sc}), because of the negligible photon loss without the light absorption of the GaAs substrate [17,18].

Heterojunction on the *p*–*n* interface is usually applied to control the built-in potential in the solar cells [19,20]. With higher bandgap heterojunction compared to the GaAs base, V_{oc} normally increases owing to the improved built-in potential. Heterojunction emitter should also have similar lattice constants (less than

~0.05% mismatch for the critical thickness larger than a few micrometers) to GaAs for the defect-free epitaxial growth [21–24]. These materials include Ga_{0.5}In_{0.5}P, Al_{0.5}In_{0.5}P, Al_xGa_{1–x}As, and (Al_xGa_{1–x})_{0.5}In_{0.5}P. Among these, Al_xGa_{1–x}As is the best candidate, owing to the largest carrier mobility (for both electrons and holes) and the lowest band offset, as listed in Table 1. Large band offset may hinder the carrier drift, leading to higher recombination rates and deteriorating solar cell performance, even though high level doping or external voltage can cause tunneling effect (detailed discussion in Section 3.1).

Moreover, the bandgap-graded layer, which can minimize the band offset at the *p*–*n* junction with GaAs, is applicable only with Al_xGa_{1–x}As. Furthermore, by considering the bandgap and lattice constant of the alloyed semiconductors, application of Al_xGa_{1–x}As allows it possible to control the band offset of the junction incorporating the bandgap-graded layer (or compositionally-graded layer).

In this study, Al_{0.3}Ga_{0.7}As heterojunction emitter was applied to increase V_{oc} , and the bandgap-graded layer was adopted for the optimum band-bending profile, leading to higher fill factor (*FF*) and thereby higher power conversion efficiency. As the Al composition (*x*) of Al_xGa_{1–x}As exceeds 0.45, the bandgap changes from direct to indirect [25], unsuitable as the absorbing layer. Moreover, for *x*=0.35–0.45, the carriers in the indirect band (*X*-valley) are more dominant than those in the direct band [26]. Therefore, Al_{0.3}Ga_{0.7}As was chosen for the heterojunction in the *p*-type emitter.

By applying both the Al_{0.3}Ga_{0.7}As heterojunction and

* Corresponding author.

E-mail address: byungwoo@snu.ac.kr (B. Park).

Table 1

Bandgap (E_g), electron affinity (χ), electron mobility (μ_e), and hole mobility (μ_h) of GaAs and several candidates for the heterojunction emitters: Ga_{0.5}In_{0.5}P, Al_{0.5}In_{0.5}P, (Al_xGa_{1-x})_{0.5}In_{0.5}P, and Al_xGa_{1-x}As [28–33]. The band energy offset of the candidate material is indicated for the GaAs base layer. The E_g , χ , μ_e , μ_h , and the band energy offset of Al_{0.3}Ga_{0.7}As employed in this study are also indicated.

Emitter materials	Bandgap (E_g) (eV)	Electron affinity (χ) (eV)	Electron mobility ^a (μ_e) (cm ² V ⁻¹ s ⁻¹)	Hole mobility ^a (μ_h) (cm ² V ⁻¹ s ⁻¹)	Energy offset (<i>n</i> -type base) (eV)	Energy offset (<i>p</i> -type base) (eV)
GaAs	1.42	4.07	8000	370	–	–
Ga _{0.5} In _{0.5} P	1.85	3.99	700	30	0.35	0.08
Al _{0.5} In _{0.5} P	2.35	3.78	100	10	0.64	0.29
(Al _x Ga _{1-x}) _{0.5} In _{0.5} P ^b	2.02–2.27	3.92–3.82	~400	~20	0.45–0.60	0.15–0.25
Al _x Ga _{1-x} As ^c	1.68–1.94	3.85–3.63	4000–800	200–100	0.04–0.08	0.22–0.44
Al _{0.3} Ga _{0.7} As	1.81	3.74	2300	150	0.06	0.33

*All data are reported at ambient temperature (~300 K) [28–33].

^a For weakly bonded condition.

^b $0.2 \leq x \leq 0.5$, where the bandgap transits from direct to indirect at $x \approx 0.53$.

^c $0.2 \leq x \leq 0.4$, where the bandgap transits from direct to indirect at $x \approx 0.45$.

compositional profile for the bandgap grading in the *n*-type light absorber, the experimental solar-cell performance was correlated to the cell parameters and recombination rates in the simulation program [27–29]. Thereby, a conversion efficiency of 28.7% was obtained, and this was only 0.1% less than that of the world-record champion cell.

2. Experimental

Each layer of the GaAs solar cell was deposited on the GaAs substrate by reacting some of the following precursors in metal-organic chemical vapor deposition (MOCVD): trimethylgallium (TMGa), arsine (AsH₃), trimethylaluminum (TMAI), phosphine (PH₃), and trimethylindium (TMIIn). Disilane (Si₂H₆) gas and diethylzinc (DEZn) as the sources of Si and Zn were used for the *n*-type and *p*-type doping layers, respectively. The bandgap-graded layers were deposited by automatically controlling the amount of the Al and Ga sources with the time during deposition in the MOCVD system.

The GaAs substrate was then removed from the deposited layer after bonding with the supporting substrate, and both electrodes were deposited by e-beam evaporation. Front electrode was additionally electroplated for minimizing the resistance with the optimized grid structure. All the solar cells were defined as the size of 1 cm² by the mesa etching, and the conversion efficiency was measured using a solar simulator (Wacom) under the standard test conditions (AM 1.5, 1 sun or 100 mW cm⁻² at 25 °C). The anti-reflective coating (ARC) layers were applied where the zinc sulfide (ZnS) and magnesium fluoride (MgF₂) were deposited by thermal evaporation with the optimized thicknesses (~50 nm and ~100 nm for ZnS and MgF₂, respectively).

For the analysis of the actual devices, the composition of Al and Ga near the *p*-*n* junction was investigated by secondary ion mass spectrometry (SIMS), cross-sectional image was analyzed by transmission electron microscopy (TEM), and crystallinity was characterized by x-ray diffraction (XRD) rocking curve.

For the heterojunction solar cell simulation, AFORS-HET, developed by Helmholtz-Zentrum Berlin (HZB), was used [27–29]. As a specialized simulation program for the devices with heterojunctions, AFORS-HET contains several options for the recombination mechanisms near the heterojunction. We tried to design the similar device structures to the experimental cell as close as possible, considering the thicknesses, stacking structure, and doping conditions of each layer. The parameters used for the simulation were adopted from elsewhere [30–36]. The device structure is quite simple (6–7 layers of III–V based materials), and the following factors were not included in the simulation: the interdiffusion of elements near the interface, the interfacial trap

density for the abrupt heterojunction, and the lattice mismatch, which may cause some discrepancies with the actual solar cells. The reflection on the front surface was not also considered in the simulation, leading to some differences in the current density and conversion efficiency in the actual cells.

3. Results and discussion

3.1. Regarding the structures of the solar cells

The Al_{0.3}Ga_{0.7}As heterojunction emitter and the bandgap-graded layer near the *p*-*n* junction were applied in the GaAs solar cells. To investigate the two above mentioned effects, several possible candidates were explored in the structure design, as schematically illustrated in Fig. 1. The *p*-type emitter can form the homojunction or heterojunction with the *n*-type GaAs base. In other words, it is GaAs 'homojunction' (Fig. 1(a)) or Al_{0.3}Ga_{0.7}As heterojunction with 'no-grade' (Fig. 1(b)). For the heterojunction, the bandgap grading can be adopted to the *n*-type GaAs base ('*n*-graded') or *p*-type Al_{0.3}Ga_{0.7}As emitter ('*p*-graded'), as shown in Fig. 1(c)–(d), to minimize the carrier recombination rate by minimizing the band offset near the *p*-*n* junction. The aluminum contents (x in Al_xGa_{1-x}As) are shown near the *p*-*n* junction (in the range of each red square) with the bandgap energy in the *n*-graded or *p*-graded solar cell, whereas the Al content and bandgap depend approximately linearly according to the Vegard's law [26].

The structures (upper two rows in Fig. 1) with the Al contents (bottom row) were applied for both the simulation and the actual device. Si and Zn were used as dopants for *n*-type and *p*-type layers, respectively (Section 2). In addition, an emitter was applied in the back of the base for all the structures, because this back-surface field increases the V_{oc} and J_{sc} by the enhanced photon recycling, especially when the bandgap of the emitter is higher than that of the base [37].

To better correlate between the simulation and experimental results, the effect of band offset on the carrier drift needs to be discussed. As mentioned in the introduction, this is tough to calculate because many variables such as doping level and external voltage need to be considered. Therefore, an alternative approach to assess the effect of band offset was proposed, by simulating our solar-cell performance based on the configuration of the applied heterojunction emitter. The band offset at the *p*-*n* interface changed by varying the electron affinity of the emitter, and the relationship between the band offset and the solar-cell parameters were investigated, as shown in Fig. 2. The FF of the simulated device decreases as the band offset increases, and it shows tiny drop when the band offset is less than ~0.3 eV. However, severe deterioration was observed for the band offset over ~0.35 eV,

دانلود مقاله



<http://daneshyari.com/article/77513>



- ✓ امکان دانلود نسخه تمام متن مقالات انگلیسی
- ✓ امکان دانلود نسخه ترجمه شده مقالات
- ✓ پذیرش سفارش ترجمه تخصصی
- ✓ امکان جستجو در آرشیو جامعی از صدها موضوع و هزاران مقاله
- ✓ امکان پرداخت اینترنتی با کلیه کارت های عضو شتاب
- ✓ دانلود فوری مقاله پس از پرداخت آنلاین
- ✓ پشتیبانی کامل خرید با بهره مندی از سیستم هوشمند رهگیری سفارشات